Solid Freeform Fabrication 2021: Proceedings of the 32nd Annual International Solid Freeform Fabrication Symposium – An Additive Manufacturing Conference
Reviewed Paper

ADDITIVE MANUFACTURING OF SI-SIC CERMETS FOR COMBUSTION DEVICE APPLICATIONS

P. P. Radyjowski, D. L. Bourell, D. Kovar and J. L. Ellzey

Walker Department of Mechanical Engineering, The University of Texas at Austin, Austin, TX 78712

Abstract

Traditional manufacturing methods for high-temperature devices are time intensive and limited to simple shapes. Additive manufacturing (AM) reduces lead times and opens the design space to more complex geometries. Indirect laser sintering of siliconized silicon carbide (Si-SiC) cermets was evaluated for creating devices compatible with combustion environments. Heat recirculating combustors especially benefit from geometric flexibility. Si-SiC process improvements are presented for the production of cermet combustors. The effect of flame on the material was studied by directly exposing samples to hot combustion products at 1000°C and 1260°C for 10 hours. Subsequently, three experimental Si-SiC combustors were manufactured and fired to evaluate the practical aspects of cermet applications. Each device was operated for 70 hours under excess-air methane flames with solid temperatures up to 1405°C. The surface oxidation and phase changes were assessed. Operating temperatures between 1200°C and 1350°C reduce damage to the material and give a promise of long-term, high-temperature operation.

Introduction

The efficiency of thermodynamic cycles is fundamentally tied to the temperature difference between hot and cold reservoirs. The extension of the operating range envelope provided by high-temperature materials improves the thermodynamic efficiency [1]. Hydrocarbon combustion, the most popular heat source, generates temperatures beyond the capabilities of common materials used to contain the reaction unless dedicated countermeasures are implemented. Several factors are important for the high-temperature selection: ultimate maximum use temperature, strength at temperature, oxidation resistance, creep behavior, and ability to withstand thermal shock. The relative importance of those factors depends on the target application [2]. Historically the common choices were high-temperature metal alloys, such as certain stainless steels and nickel-based superalloys. Their popularity stems from good strength and toughness combined with relative ease of machining. Unsurprisingly, high-temperature metal parts fabrication has dominated the space of additive manufacturing (AM) for high-temperature applications. General Electric and Siemens extensively use AM processes in gas turbine combustor manufacturing to reduce the part count of complex assemblies, improve performance, and simplify operations [3, 4]. A 2020 NASEM report on advanced technologies for gas turbines identified AM as a high-priority research area crucial for furthering development in the next decade [5]. However, the metal-based materials are limited to approximately 1200°C, which thermally constrains many designs and impacts device performance. A noteworthy example is an intricate combustor cooling design, fundamentally enabled by AM, that purposely increases the heat loss to keep the material temperature within operational limits [6]. This case represents a deliberate efficiency reduction dictated by materials constraints.

Low-stress devices, such as combustors and heat exchangers, do not require high strength. Therefore the goal for high-temperature material in such application is to withstand the highest possible temperature for the longest time [7]. Technical ceramics are promising materials in such uses due to their elevated operational temperatures. However, the implementation of ceramics materials has been restricted due to their brittle nature and complicated shaping processes. The traditional manufacturing methods, such as mold pressing or slurry deposition, have significant limitations on the final part shape. Furthermore, complex ceramic shapes are usually avoided due to the great difficulty of associated machining. Therefore intricate multi-component assemblies are required. A range of AM methods could address this issue as the ceramic part would be created in the final, complex shape. For example, Sobhani *et al.* [8] used stereolithography to produce tailored microporous ceramic media for low emission combustors. Precise control over the macrostructure improved the performance by position-dependent regulation of the effective thermal conductivity. Furthermore, AM's ability to reliably create intricate geometries with millimeter-scale features opens new possibilities for sophisticated designs that can be produced with greater tolerance and less manual labor.

This study examines the applicability of AM materials for combustion device applications. Combustors were chosen due to the utilization of high-temperature chemistry while being limited by material properties and suitable manufacturing methods. Increased operating temperatures used to be achieved either by incorporating bulk-manufactured ceramics that severely constrain possible geometries or by complex metal designs that employed intricate heat transfer patterns to lower the surface temperatures to acceptable levels. AM manufactured material presented in this work provides higher temperature compatibility without sacrificing shape reproduction capabilities. The combustor that significantly benefits from such improvement is the heat recirculating reactor (HRR), which recycles the heat energy from hot products back into incoming reactants. The required heat transfer conditions necessitate narrow passages, non-trivial geometries, and direct exposure of solid to the flame [9]. HRR devices are severely constrained either by insufficient temperature limits of metals or the restricted complexity of handcrafted assemblies made from pre-made simple shape high-temperature ceramics. AM also increases dimensional tolerances and reduces the time and manual labor required for handcrafted assemblies. The ability to reliably and repeatedly create intricate geometries with millimeter-scale features opens new possibilities for sophisticated designs and innovative applications. The specific HRR type used in this study is a four-channel counterflow layout, originally created by hand in zirconia and SiC ceramics [10]. It showed extended flammability limits when used as a combustor and could also be used as a fuel reformer or a thermal oxidizer. However, further optimizations and industrial applications were limited due to manufacturing difficulties.

Methods

Indirect Laser Sintering of Si-SiC

Indirect laser sintering with metal infiltration was first developed at The University of Texas at Austin [11, 12] to produce dimensionally stable yet fully dense ceramic parts. The material of choice was silicon carbide (SiC) infiltrated with silicon (Si) metalloid, which results in a ceramic-metal composite called cermet. The high melting point of Si combined with the excellent high-temperature properties of SiC makes this cermet applicable for combustion applications. A detailed process diagram for siliconized silicon carbide (Si-SiC) manufacturing is illustrated in Figure 1. First, the pure ceramic powder is mixed with a temporary binder compatible with the laser sintering (LS) process (Figure 1a). Only the phenolic binder is activated during the AM step,

which holds ceramic particles together to produce a green part (Figure 1b). The temporary binder used in this study, partially polymerized phenolic resin (novolac GP-5546, Georgia Pacific Chemicals, Atlanta GA, United States), allows multiple remelting, which is a crucial characteristic for the LS process. Upon completion, the green part is retrieved from the powder bed via mechanical methods. Excavation is a delicate operation as the bonding strength of the binder at this stage is very low. Subsequently, the phenolic binder undergoes a thermally induced polymerization (crosslinking) to prevent further melting at higher temperatures (Figure 1c), hence preserving the part shape. Inconveniently, the polymerization occurs at temperatures above 90°C, beyond the resin's softening point. As a result, the part experiences shrinkage in the vertical direction and deformation of unsupported sections due to gravity. The influence of thermal processing in the crosslinking process was examined using a set of thin 100×20×2 mm samples bridged over a 38 mm wide unsupported section, as shown in Figure 6.

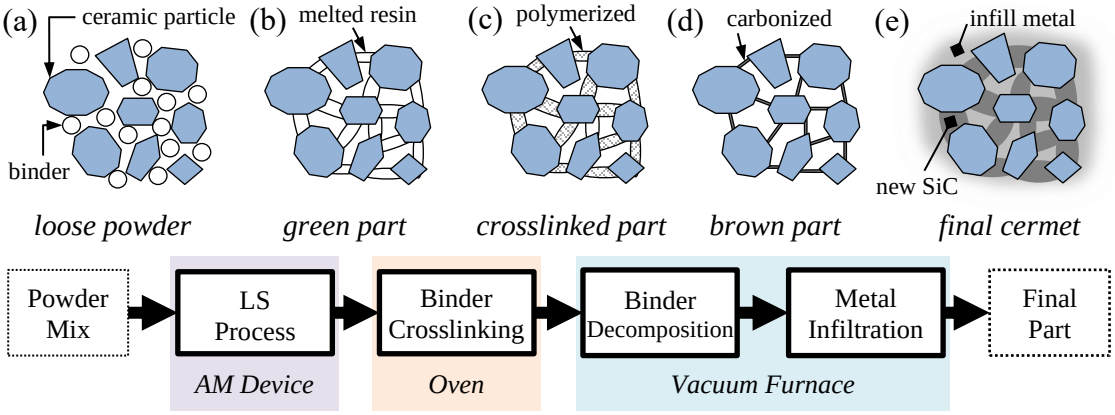

Figure 1. Schematic of AM Si-SiC process: indirect laser sintering with metal infiltration

The crosslinked green state is the most suitable form for modification, such as drilling holes or manual wall carvings. The part then undergoes a burn-out step, where the binder is carbonized into carbon bridges (Figure 1d). This process takes place in the vacuum furnace at a maximum temperature of 900°C. The result is a porous ceramic preform, generally referred to as a brown part. The traditional approach would proceed with high-temperature direct sintering of ceramic particles. While a part produced using this approach would have intrinsic properties of the neat ceramic, it would also experience significant volumetric shrinkage (>10%), with resulting substantial distortions. Instead of direct sintering, the part is infiltrated with a suitable substance to avoid shrinkage (Figure 1e). For the infiltration step, the brown part is surrounded by pieces of pure silicon and returned to the vacuum furnace, where metalloid melts and wicks into the ceramic structure. The favorable wetting interaction of the Si - SiC pair provides the capillary driving pressure further aided by the vacuum environment. Uniquely for the Si - SiC system, when molten silicon contacts the carbonized binder residue, more silicon carbide is produced by a reaction between the Si and the carbon. This reaction further increases the ceramic-to-metal ratio of the final part. There is usually no need for machining, and only minimal assembly is required to interface with the external equipment. Since the infiltrant flows into the voids and there is no physical force at play, only a small shape change occurs relative to the brown part.

Direct Flame Exposure

The direct flame exposure experiment was designed to investigate the longevity of Si-SiC cermet under an excess-air flame. The Si-SiC samples were suspended on a Nichrome wire above a ceramic flat flame burner, further described in Smith *et al.* [13]. The coupon was positioned such that the flame impinged at its bottom surface, as shown in Figure 2. The apparatus maintained a stable temperature and flame position near the sample for the period of the experiment. A single K-type thermocouple measured the temperature at the middle of sample height (≈ 5 mm above the flame) with flow conditions actively adjusted to maintain the desired conditions.

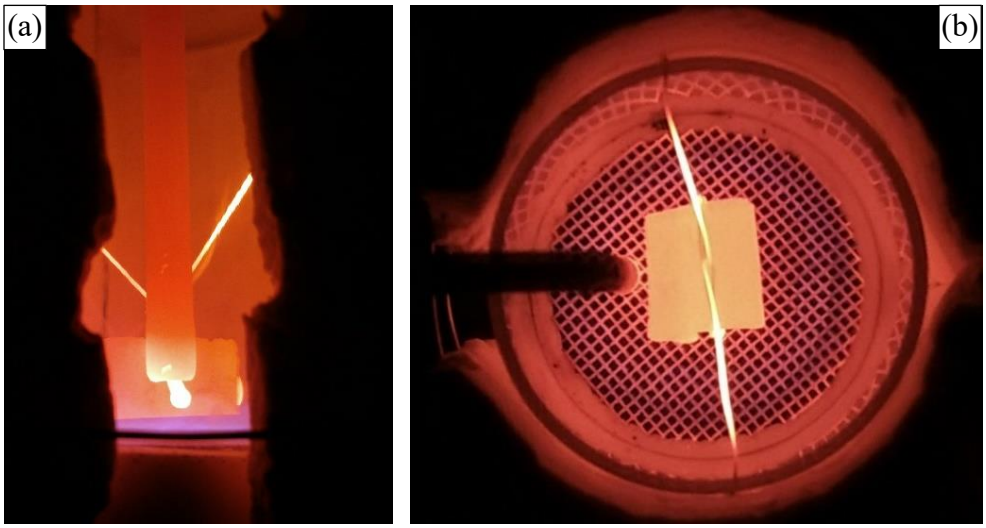

Figure 2. Flame exposure apparatus for AM Si-SiC samples: a) side view b) top view

Two temperature levels were studied representative of practical, lean combustion applications: a lower 1000°C temperature with higher oxygen content and a 1260°C flame closer to a stoichiometric mixture. Both air and fuel streams were simultaneously stopped at the end of the test, allowing the sample to cool via natural convection. The experiment was performed in 5-hour increments for a total of 10 hours. After each exposure, the sample was weighed on a precision laboratory scale (±0.5 mg), and the volume was measured using a water displacement method. Furthermore, optical inspection, scanning electron microscope (SEM) imaging, and energy-dispersive spectroscopy (EDS) analysis were performed after 10 hours of exposure to investigate the oxidation damage.

Si-SiC Combustors

The counterflow HRR combustor design was reproduced in AM Si-SiC using the process described in the Indirect Laser Sintering of Si-SiC section above. The internal geometries of created parts are shown in Figure 3. The previous handcrafted version, used as a reference point for new devices, was limited to simple straight channels, translating into the current AM straight channel pattern (Figure 3a). The freeform capabilities of AM process enabled modifications to channel shape, which opened new unique research possibilities. A study on the effect of convective heat transfer on combustion characteristics was performed using two modified designs: an AM diverging channel (Figure 3b) and an AM split-channel (Figure 3c). All reactors used a 2 mm separating wall, and the narrowest channel width of 3 mm was achieved in the AM split-wall device. Furthermore, the smallest resolved features were 1 mm 45° chamfers and 1 mm radius fillets on the leading edges of the splitter wall in the AM split-channel reactor. The presented

feature sizes are LS machine-specific, with other teams successfully achieving a microfeature reproduction [14]. The finished AM Si-SiC parts were instrumented, linked with a precise flow delivery system, and operated with flames present for extended periods of time. Figure 4 shows the AM diverging reactor under a stable operation with external insulation removed.

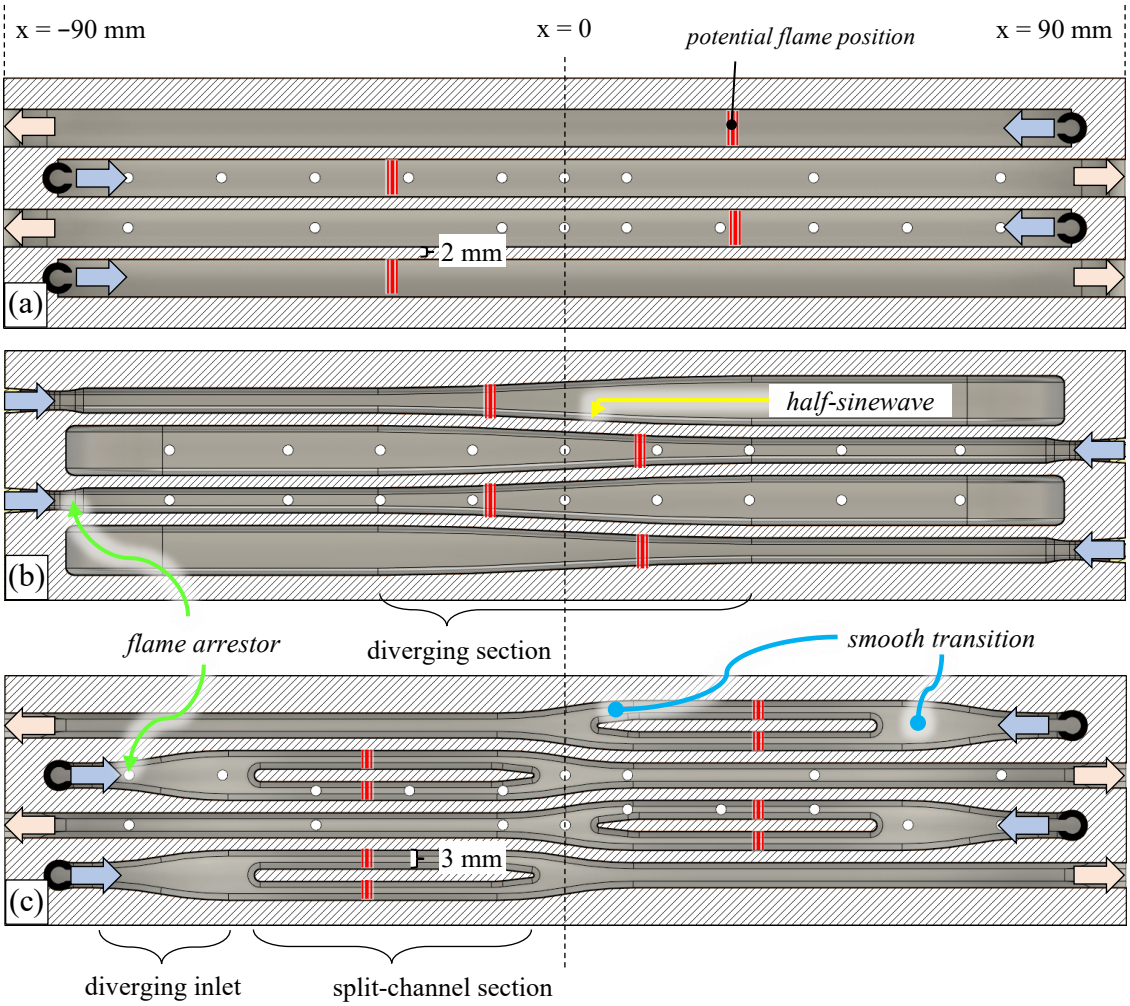

Figure 3. The internal structure of AM Si-SiC combustors: a) AM straight channel design, b) AM diverging channel design, and c) AM split-channel design

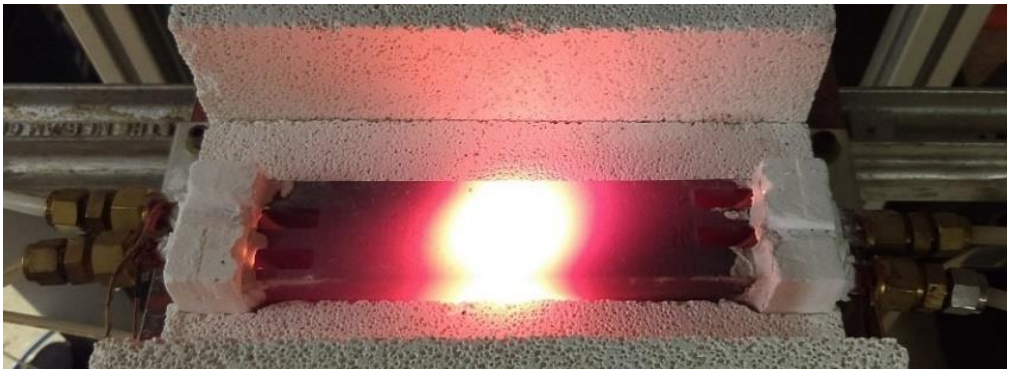

Figure 4. AM combustion reactor under operation with upper insulation removed, so the containing flame section is visible.

Results

Indirect Laser Sintering of Si-SiC

The relative size changes compared with the CAD model were tracked through the manufacturing process and compiled in Figure 5. The CAD-green step involving the LS processing showed a 3% dimensional increase in the layer X-Y plane and 2% growth in the cross-layer Z direction. This change is a stable feature of the laser sintering process usually accounted for by the software prescaling that is known once the procedure is established and characterized. The subsequent 1% decrease in X-Y was close to the measurement uncertainty. However, a substantial 4% reduction in the vertical Z direction registered between green and brown stages was associated with the crosslinking step. Ultimately, the final volumetric change thorough the process is significantly lower than traditional ceramic densification methods (>10%).

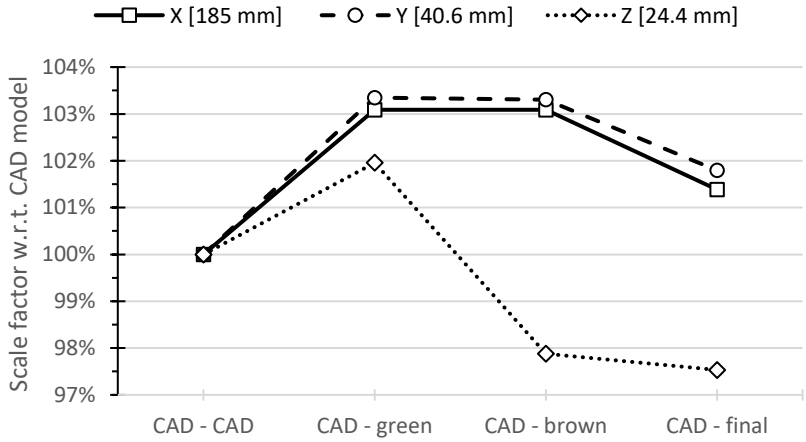

Figure 5. Geometry changes along various stages of the Si-SiC process in planar (X, Y) and vertical stacking (Z) directions.

The result of the further deformation test during the crosslinking processing is shown in Figure 6. Two approaches were studied: a fast thermal shock and a slow temperature ramp. The shock test (Figure 6a) minimized the polymerization time by directly exposing the part to high temperatures. In this case, the bridge collapsed as the polymerization process was not fast enough to counteract the viscous flow. The new approach (Figure 6b) used in this study uses a slow temperature ramp to allow partial polymerization before substantial softening occurs. A stair-step temperature profile approximated a 1.25°C/hour ramp over 40 hours and was followed by a sharp increase in temperature followed by a hold at 250°C. The resulting deformation was substantially lower, although the required time increased significantly. Prior to this work, the shock crosslinking procedure was commonly used in combination with additional support, either external (sand embedding) or internal (low viscosity epoxy resin infiltration). The slow ramp approach provided a more straightforward alternative with substantially reduced deformation. However, since the deformation is not entirely prevented, as seen for Z direction in Figure 5, additional support might still be required for dimension-critical parts.

Besides the deformation, the Si-SiC process is prone to incomplete infiltration, shown in Figure 7a. This is caused by either a locally insufficient amount of infiltrant or blocking of capillary paths by newly created SiC, as described by Song *et al.* [15]. Therefore, repetitive remelting with additional silicon was required until the desired density and close porosity were achieved.

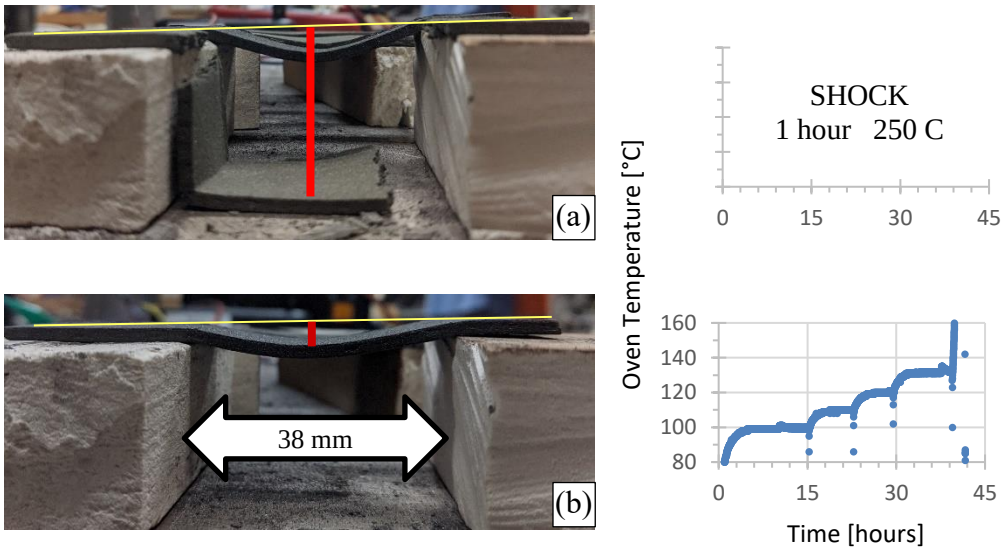

Figure 6. Unsupported bridge deformation in the crosslinking step: a) fast shock method b) 2-temperature approach c) approximated temperature ramp

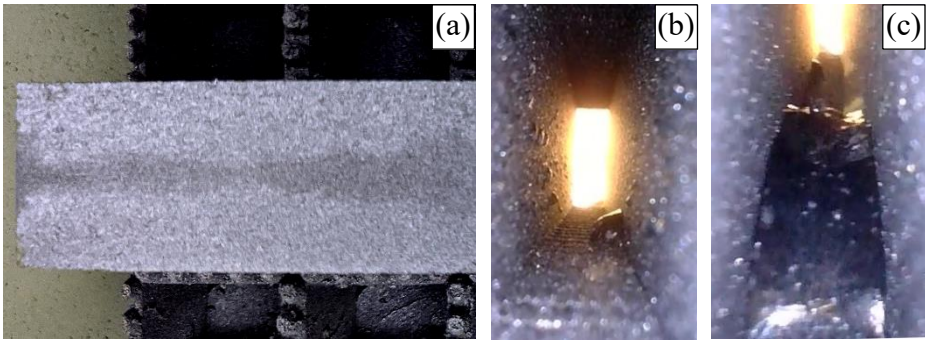

Figure 7. Examples of process imperfections: a) incomplete infiltration, contrast-enhanced b) Si protrusions in a channel of Si-SiC c) Si pooling in a channel of Si-SiC

However, the amount of infiltrant had to be carefully controlled, as excessive silicon tends to protrude from the part surface after solidification, Figure 7b. Si pooling can also occur in severe cases of over-infiltration, Figure 7c. The cause was identified by Stevinson *et al.* [16], who showed that the positive volume change upon solidification of Si causes excess metal to squeeze out of the structure as it solidifies.

Direct Flame Exposure

The results of the direct flame exposure experiment are summarized in Table 1. The mass and volume history shows that the initial 5-hour exposure caused a mass loss with a volume gain in both cases. The positive volume change is associated with the formation of less dense SiO_2. The observed mass loss was more pronounced at higher temperatures despite a lower oxygen content in the combustion atmosphere. After another 5 hours, the sample tested at 1260°C experienced a small mass gain accompanied by further volume increase, indicating passive oxidation. This type of oxidation is beneficial for the long-term material life as the growing oxide layer forms a diffusive barrier that substantially limits further deterioration. This behavior agrees with Ernstberger's findings [17] that Si-SiC experiences passive oxidation after the initial period of

mass loss, even at low oxygen concentrations. Meanwhile, the sample tested at 1000°C continued to lose mass after 10 hours, combined with a net volume decrease. This behavior indicated undesirable active oxidation and progressive deterioration of the material occurring at 1000°C

Temperature	Time	Mass change (total) ± 0.02%	Volume change (total) ± 2%
25°C (reference)	0 hr	0.00%	0%
1000°C	5 hr	- 0.12%	+ 6%
1000°C	10 hr	- 0.14%	- 1%
1260°C	5 hr	- 0.17%	+ 4%
1260°C	10 hr	- 0.14%	+ 12%

Table 1. Summary of the total mass and volume changes due to flame exposure.

The outcomes of optical inspection, SEM imaging, and EDS analysis after 10 hours of exposure are compiled in Figure 8. The front surface of the low-temperature part is cracked with a spalling taking place, which explains the recorded mass loss. Furthermore, the SEM image of the 1000°C sample showed angular oxide structures poorly attached to the surface. In contrast, the high-temperature sample contained a smooth and well-integrated SiO_2 oxide cover. The difference in SiO_2 morphology can be explained by its glass transition temperature of approximately 1200°C. For the sample tested at 1000°C, the oxide behaved as a crystalline solid leading to the surface spalling and active oxidation. Meanwhile, the sample tested at a higher temperature was covered in the amorphous form of SiO_2, which bonded well to the underlying cermet. The EDS analysis of both surfaces further confirmed a higher oxygen concentration in the sample tested at 1260°C despite the lack of visible damage and a lower oxygen concentration in this flow environment. Meanwhile, the low-temperature sample showed a lower oxygen content because most of the SiO_2 was removed from the part by spalling.

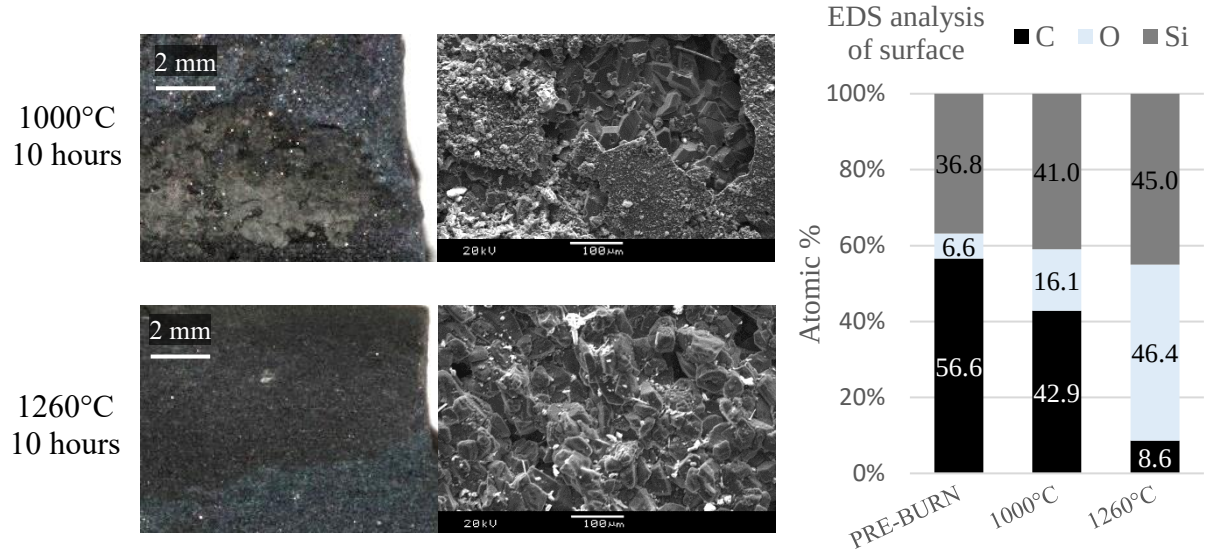

Figure 8. Optical (left) and SEM (center) images of samples after a 10-hour exposure at 1000˚C (top) and 1260˚C (bottom). The outcome of the EDS analysis is shown on the right.

Therefore, if a lower temperature operation is desired, an intentional passivation step during the manufacturing process could be added to grow a well-anchored protective layer. Such layer should not experience severe spalling issues at lower temperatures and would therefore extend the part lifetime.

Si-SiC Combustors

All three AM combustors operated in a stable fashion through the entire set of experimental activities required to collect the lean combustion performance data. Detailed combustion results are presented elsewhere [18, 19]. Each reactor experienced at least 70 hours of operation with ten complete cool-down and warm-up cycles and remained fully operational. In contrast, previous handmade devices exhibited microcracks in the ceramic due to excessive thermal stresses. The three AM reactors studied showed no structural issues with high thermal gradients, even as the flame impinged on the cold, room-temperature wall during the startup period. Internal surfaces were inspected visually via a borescope video probe at regular time intervals. The surface degradation of the AM straight channel reactor at the section experiencing the highest temperature is shown in Figure 9. The remaining reactors exhibited similar behavior and therefore are not presented. Within the first 5 hours, protrusions appeared in the hottest part of the channel. After 5 hours, the initial stage of protrusion formation was characterized by smooth, metallic skin. By the 10-hour mark, a significant amount of new growth could be observed. At this point, all channels were mechanically cleaned since the protrusion meaningfully obstructed the flow. During the remainder of the experiments (10 to 70 hour period), only the SiO_2 oxide spalling was observed with no further protrusion growth. This degradation mode was consistent with the observations made on samples tested at lower temperatures under direct flame exposure, discussed in the previous section.

The generation of solid 0.2 - 4 mm chunks within the channels is an issue for practical applications. A prolonged exposure caused further growth into an irregular shape and an opaque appearance. Notably, this occurred only in the hottest section of the channel, yet at temperatures below the melting point of pure Si metalloid (1414°C). A representative sample was recovered and inspected under the SEM, with results compiled in Figure 10.

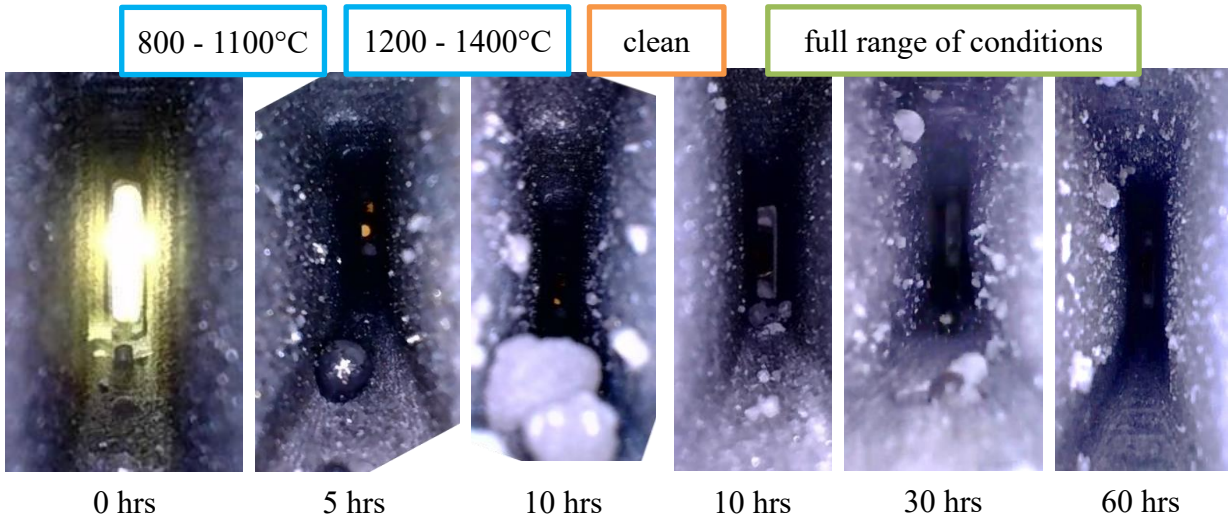

Figure 9. Wall damage as observed from within a channel in an AM straight combustor. Mechanical cleaning was performed at 10 hours.

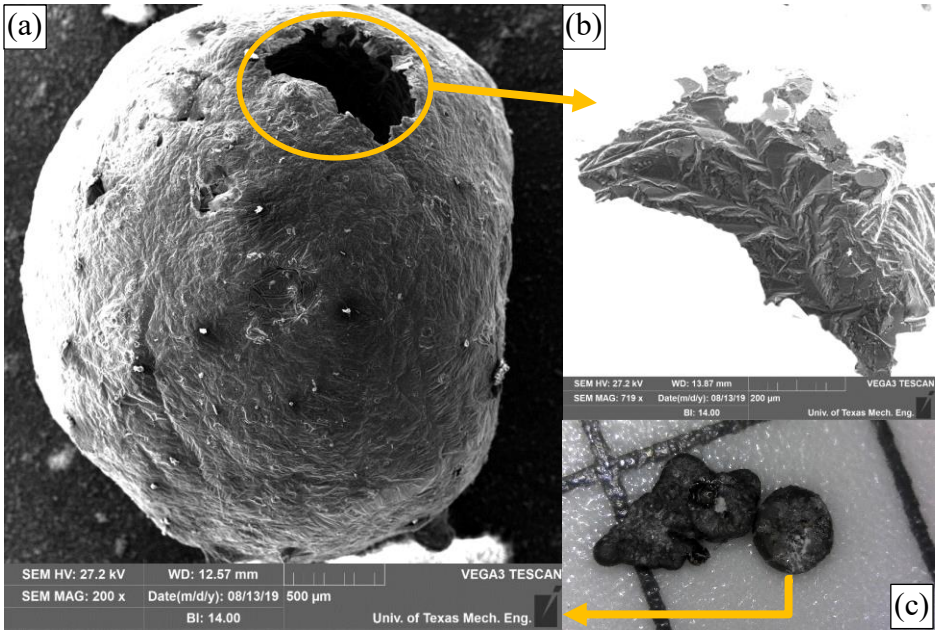

Figure 10. Combustion-induced protrusion: a) SEM overview b) SEM view of a crevice in oxide skin c) optical view on 10×10 mm hatch pattern

The outer surface is a smooth oxide skin, akin to the observation made on the sample tested at high temperature under direct flame exposure. The cavity in the upper end of the object was a suitable target for EDS. The analysis showed a significant prevalence (>80 at%) of silicon. Furthermore, an overexposed image of the shaded area of the cavity, Figure 10b, shows surface features characteristic of metallic substance. Rezaeia *et al.* [20] reported similar silicon bead formation for Si-SiC lattice samples after a 1-hour hold in a 1400°C air atmosphere. According to their findings, the local concentration of impurities in the Si phase depressed the newly formed alloy's melting point below the surrounding conditions. The silicon shrunk upon melting, which facilitated the oxidation within the structure via opened micropores. Subsequently, a formation of sub-surface, low-density SiO_2 led to an increase of the internal stresses that squeezed the molten silicon alloy into the surface. Finally, the low wettability of silicon on SiO_2 causes beading and coalescence into larger globules. The described process may be detrimental to the long-term lifetime of the material since expelled metal leaves open porosity that further accelerates the oxidation process. The formation and spalling of SiO_2 were observed in the experimental reactors at the 30 and 60 hours marks in Figure 9. Nevertheless, the surface degradation was minor compared to wall thickness allowing for successful operation throughout the testing period.

Conclusions

The Si-SiC cermet created via indirect laser sintering was investigated for combustion device use. High-temperature and combustion applications are attractive fields for AM manufacturing. The freeform fabrication of parts with operational limits beyond current materials opens new possibilities in the field of combustion. Direct flame exposure tests at 1000°C and 1260°C confirmed the high-temperature compatibility of the studied cermet. The obtained data shows that long-term use of Si-SiC is possible for operational temperatures above the glass transformation temperature of SiO_2 (≈1200°C) due to the formation of a passivation barrier. Subsequently, a practical application using a heat recirculating counterflow combustor was

investigated. Three devices were produced in Si-SiC containing various degrees of complexity with the smallest feature size of 1 mm. All devices were tested for at least 70 hours and remained fully operational afterward. The combustion tests performed on AM Si-SiC reactors showed the material suitable for practical combustion applications at temperatures up to 1400°C. The geometric flexibility provided by AM enabled new, unique combustion research opportunities. The wall damage through the experiments showed previously observed SiO_2 flakes formation accompanied by Si metalloid beads formation at higher temperatures. This process may be detrimental to the long-term longevity of the material and reduce the material's upper-temperature limit. However, the overall performance of AM-based Si-SiC is favorable for combustion applications and opens new design possibilities.

References

[1] G. W. Meetham, "High-temperature materials - a general review," *J. Mater. Sci.,* vol. 26, pp. 853-860, 1991.

[2] J. R. Davis, Heat-resistant materials, Materials Park, Ohio: ASM International, 1997.

[3] D. Appleyard, "Powering up on powder technology," *Met. Powder Rep.,* vol. 70, no. 6, pp. 285-289, 2015.

[4] R. Huff and T. T. Wohlers, "Redesigned for Additive Manufacturing: Serial production of a new fuel swirler for Siemens gas turbine," *Metal AM,* vol. 5, no. 3, pp. 169-172, 2019.

[5] Natl. Acad. of Sciences, Engineering, and Medicine, "Advanced Technologies for Gas Turbines," The National Academies Press, Washington, DC, 2020.

[6] A. Adamou and C. Copeland, "Experimental and Computational Analysis of Additive Manufactured Augmented Backside Liner Cooling Surfaces for Use in Micro-Gas Turbines," *ASME J. Turbomach.,* vol. 143, p. 071012, 2021.

[7] Y. Bar-Cohen, High temperature materials and mechanisms, 1st ed., Boca Raton, Florida: CRC Press, 2014.

[8] S. Sobhani, S. Allan, P. Muhunthan, E. Boigne and M. Ihme, "Additive Manufacturing of Tailored Macroporous Ceramic Structures for High-Temperature Applications," *Adv. Eng. Mater.,* vol. 22, p. 2000158, 2020.

[9] J. L. Ellzey, E. L. Belmont and C. H. Smith, "Heat recirculating reactors: Fundamental research and applications," *Prog. Energy Combust. Sci.,* vol. 72, pp. 32-58, 2019.

[10] I. Schoegl and J. L. Ellzey, "A mesoscale fuel reformer to produce syngas in portable power systems," *Proc. Combust. Inst.,* vol. 32, pp. 3223-3230, 2009.

[11] R. S. Evans, D. J. Bourell, J. J. Beaman and M. I. Campbell, "Reaction bonded silicon carbide: SFF, process refinement and applications," in *2003 Int. Solid Freeform Fabr. Symp. Proc.*, Austin, 2003.

[12] B. Y. Stevinson, D. J. Bourell and J. J. Beaman, "Support-Free Infiltration of Selective Laser Sintered (SLS) Silicon Carbide Preforms," in *2006 Int. Solid Freeform Fabr. Symp. Proc.*, Austin, 2006.

[13] C. H. Smith, D. I. Pineda and J. L. Ellzey, "Syngas production from burner-stabilized methane/air flames: The effect of preheated reactants," *Combust. Flame,* vol. 160, no. 3, pp. 557-564, 2013.

[14] A. Streek , P. Regenfuss, F. Ullmann, L. Hartwig, R. Ebert and H. Exner, "Processing of silicon carbide by laser micro sintering," in *2006 Int. Solid Freeform Fabr. Symp. Proc.*, Austin, 2006.

[15] S. Song, Z. Gao, B. Lu, C. Bao, B. Zheng and L. Wang, "Performance optimization of complicated structural SiC/Si composite ceramics prepared by selective laser sintering," *Ceram. Int.,* vol. 46, no. 1, pp. 568-575, 2020.

[16] B. Stevinson, D. Bourell and J. Beaman, "Over-infiltration mechanisms in selective laser sintered Si/SiC preforms," *Rapid Prototyp. J.,* vol. 14, pp. 149-154, 5 2008.

[17] U. Ernstberger, H. Cohrt, F. Porz and F. Thummler, "Oxidation von Silizium-infiltriertem Siliziumkarbid," *Berichte der DKG,* vol. 60, pp. 167-173, 1983.

[18] P. P. Radyjowski, I. Schoegl and J. L. Ellzey, "Experimental and Analytical Investigation of a Counterflow Reactor at Lean Conditions," *Combust. Sci. Technol.,* 2021.

[19] P. P. Radyjowski and J. L. Ellzey, "Experimental Study on the Influence of Gas-Solid Heat Transfer in a Mesoscale Counterflow Combustor," *Combust. Sci. Technol. (under review),* 2021.

[20] E. Rezaeia, S. Haussener, S. Gianella and A. Ortona, "Early-stage oxidation behavior at high temperatures of SiSiC cellular architectures in a porous burner," *Ceram. Int.,* vol. 42, no. 14, pp. 16255-16261, 2016.